JACS Au
AN OPEN ACCESS JOURNAL OF THE AMERICAN CHEMICAL SOCIETY

pubs.acs.org/jacsau
Article

Cell-Permeable Fluorescent Sensors Enable Rapid Live Cell Visualization of Plasma Membrane and Nuclear PIP3 Pools

Rajasree Kundu, Sahil Kumar, Amitava Chandra, and Ankona Datta*

Cite This: JACS Au 2024, 4, 1004−1017
Read Online

ACCESS | Metrics & More | Article Recommendations | Supporting Information

ABSTRACT: Phosphoinositides, phospholipids that are key cell-signal mediators, are present at very low levels in cellular membranes and within nuclei. Phosphatidylinositol-(3,4,5)-trisphosphate (PIP3), a phosphoinositide barely present in resting cell membranes, is produced when cells receive either growth, proliferation, or movement signals. Aberrant PIP3 levels are associated with the formation of cancers. PIP3 pools are also present in the nucleus, specifically in the nucleolus. However, questions related to the organization and function of this lipid in such membraneless intranuclear structures remain unanswered. Therefore, chemical sensors for tracking cellular PIP3 are invaluable not only for timing signal initiation in membranes but also for identifying the organization and function of membraneless nuclear PIP3 pools. Because PIP3 is present in the inner leaflet of cell membranes and in the nucleus, cell-permeable, rapid-response fluorescent sensors would be ideal. We have designed two peptide-based, water-soluble, cell-permeable, ratiometric PIP3 sensors named as **MFR-K17H** and **DAN-NG-H12G**. **MFR-K17H** rapidly entered into the cell cytoplasm, distinctly reporting rapid (<1 min) time scales of growth factor-stimulated PIP3 generation and depletion within cell membranes in living cells. Importantly, **MFR-K17H** lighted up inherently high levels of PIP3 in triple-negative breast cancer cell membranes, implying future applications in the detection of enhanced PIP3 levels in cancerous cells. On the other hand, **DAN-NG-H12G** targeted intranuclear PIP3 pools, revealing that within membraneless structures, PIP3 resided in a hydrophobic environment. Together, both probes form a unique orthogonally targeted combination of cell-permeable, ratiometric probes that, unlike previous cell-impermeable protein-based sensors, are easy to apply and provide an unprecedented handle into PIP3-mediated cellular processes.

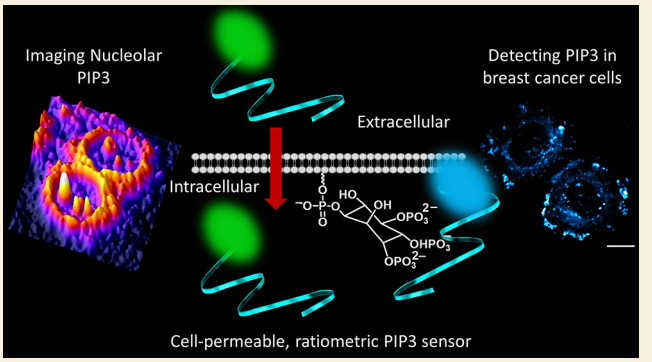

KEYWORDS: *cell-permeable PIP3 sensor, imaging nuclear PIP3 pool, imaging PIP3 dynamics, phosphoinositide sensor, ratiometric PIP3 sensor, fluorescent PIP3 sensor, peptide-based PIP3 sensor*

INTRODUCTION

Phosphatidylinositol-3,4,5-trisphosphate (PIP3) (Figure S1) is a transient phospholipid present in the inner leaflet of eukaryotic cell membranes.[1−3] Breakthrough studies around 2006 identified the presence of PIP3 also within the nucleus, specifically in the nucleolus.[4,5] In the resting state of the cell, the concentration of this lipid is extremely low and estimated to be around 50 nM with possibly higher ∼5 μM local concentrations in parts of the membrane.[6] Upon external chemical stimulation, for example, with growth factors, the concentration of PIP3 increases to 2 μM levels, with local concentrations as high as ∼200 μM in the plasma membrane.[6] In the cell membrane, PIP3 is the central lipid that mediates cell growth, proliferation, and movement.[6−8] In this context, PIP3 is a singularly important lipid that controls healthy versus cancerous cell growth (Figure S2).[9−12] The enzymes phosphatidylinositol-3-kinases (PI3Ks) synthesize PIP3 on the cell membrane by phosphorylating phosphatidylinositol-4,5-bisphosphate (PI(4,5)P2) (Figure S1), a lipid which is constitutively present in the inner leaflet of the plasma membrane (Figure S2(A)).[3,13] PI3Ks act in response to growth stimuli.[14−16] Increased levels of PIP3 mediate the activation of protein kinases like Akt, which participate in transmitting cell growth and proliferation signals.[3,9−11,16] The enzyme phosphatase and tensin homolog (PTEN) converts PIP3 back to PI(4,5)P2 and maintains the levels of PIP3 in healthy cells to allow normal cell growth and proliferation (Figure S2-(A)).[3,4,17,18] Hyperactivated PI3Ks and deactivated PTEN lead to increase in PIP3 levels causing uncontrolled cell proliferation (Figure S2(B)).[9−12,16,18−22] Activating mutations in PI3Ks and deactivating mutations in PTEN are prevalent in cancers[9,10,12,19,22] and mutant PI3Ks are found in 30−40%

Received: November 21, 2023
Revised: February 16, 2024
Accepted: February 20, 2024
Published: March 13, 2024

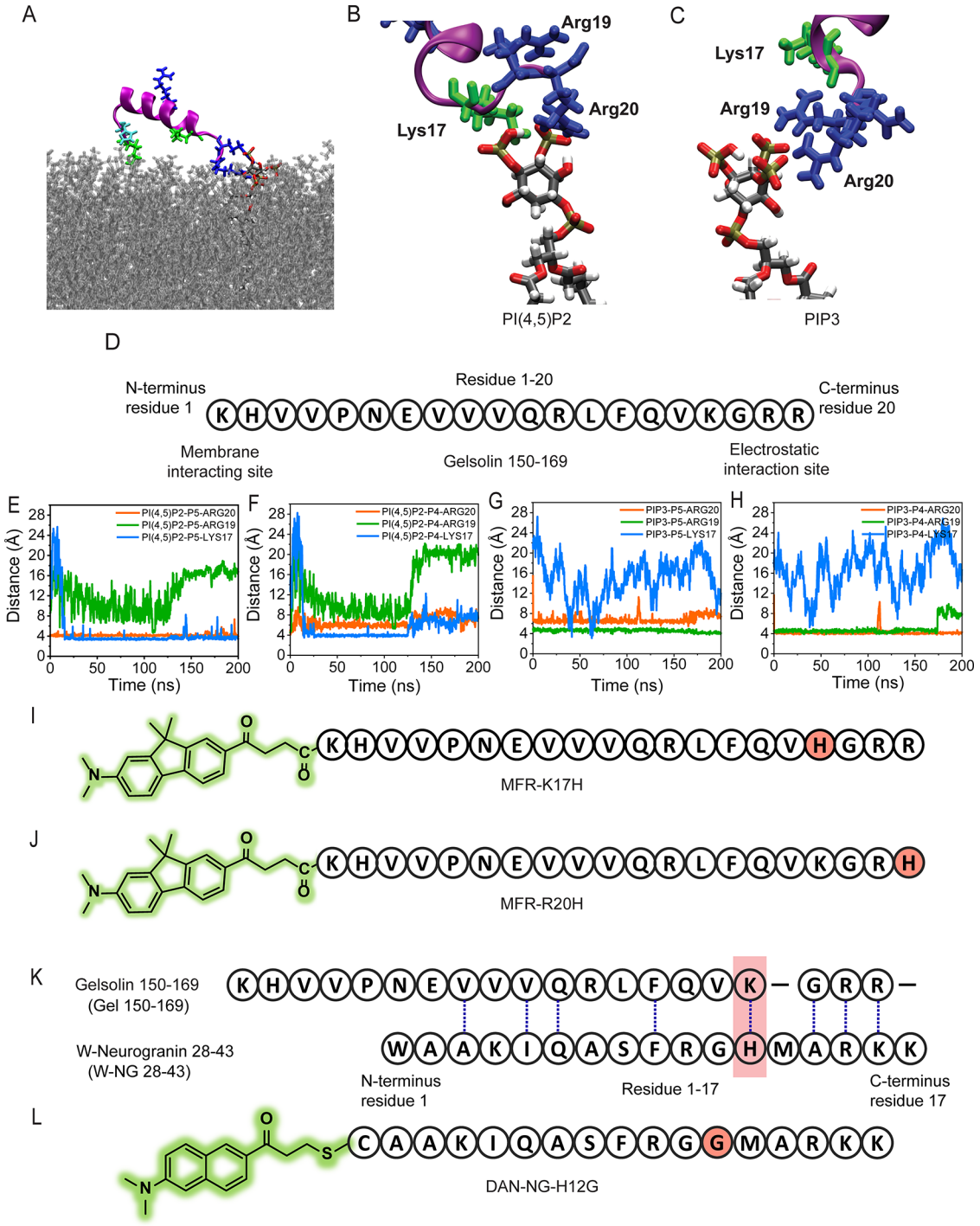

Figure 1. Design of cell-permeable, fluorescent PIP3 sensors. (A) Snapshot from MD simulation showing the interaction of gelsolin 150−169 (peptide: violet) with a PIP3 molecule (gray licorice; phosphate-oxygen-atoms: red) in a POPC (silver) lipid bilayer. Cationic amino acids on the peptide are shown using licorice model representation: Arg (blue), His (cyan), and Lys (green). (B, C) MD snapshot highlighting the interactions of the positively charged amino acids in the C-terminus of the peptide with PI(4,5)P2 and PIP3 headgroups, respectively. (D) Sequence of Gel 150−169 and residue numbering from N-terminus to C-terminus used in this paper. Distances of the charged moiety on cationic residues, Arg 20, Arg 19, and Lys 17 within Gel 150−169, to (E) the 5-phosphate group of PI(4,5)P2; (F) the 4-phosphate group of PI(4,5)P2; (G) the 5-phosphate group of PIP3; and (H) the 4-phosphate group of PIP3; throughout 200 ns MD simulation runs. Chemical representations of peptide-based fluorescent sensor **MFR-K17H** (I) and control molecule **MFR-R20H** (J). (K) Peptide sequence alignment of Gel 150−169 and W-NG 28−43 showing alignment of K17 in Gel 150−169 with H12 in W-NG 28−43. (L) Chemical representation of peptide-based fluorescent sensor **DAN-NG-H12G**.

cancer patients, especially in breast cancer.[10,16,23] Further, the synthesis of membrane PIP3 in the front-end of chemotaxing cells leads to actin polymerization, which directs cell migration.[7,24]

While the roles of PIP3 in the cell membrane are reasonably well-established and putative concentrations estimated, the nuclear PIP3 pool has remained elusive.[4,25,26] Anti-PIP3 antibody staining studies have provided definite evidence for the presence of PIP3 within nucleoli.[27] Recent interactomics

https://doi.org/10.1021/jacsau.3c00738
JACS Au 2024, 4, 1004−1017

studies showed that nuclear PIP3 interacted with proteins enriched in RNA and DNA binding domains.[27] These proteins spanned functions including RNA processing, cytokinesis, protein folding, and DNA repair.[27,28] Proteins involved in cell survival and proliferation, like PI3Ks, were also identified.[5] Both the plasma membrane and the nuclear PIP3 pools play roles in tumorigenesis, perhaps through a common PI3K link.[5,29,30] However, the exact roles of nuclear PIP3 are still unknown.[25] Importantly, the organization of PIP3 in nonmembranous environments within the nucleus, especially the nucleolus, is unclear.[27,31] It is hypothesized that the acyl chains might be sheltered from the aqueous environment, but this has not been demonstrated thus far.[27,31]

In this backdrop, cell-permeable, fluorescent chemical sensors for imaging and tracking PIP3 can provide key information on the fundamental basis of PIP3-mediated cell-signaling pathways and importantly provide the yet unavailable handle for studying the nuclear pool. Moreover, PIP3 levels are elevated in several forms of cancer, but methods to detect PIP3 in intact cancer cells for rapid diagnostics are unavailable due to the lack of cell-permeable, rapid-response PIP3 sensors.[20] Hence, such a sensor can also pave the path for the development of rapid assays to measure PIP3 levels in cancer cells and guide appropriate therapy, for example, the use of PI3K inhibitors.[9−11,32]

All PIP3 sensors reported to date are protein-based, cell-impermeable biosensors (Table S1).[33−39] These sensors have been generated either by encoding the genes of fluorescent proteins with the gene of a PIP3 binding protein domain or by conjugating an organic dye directly to a PIP3 binding protein.[3,35] Genetically encoded probes that have been developed for sensing PIP3 are of two types: nonresponsive fluorescent protein-tagged probes[36−38] and responsive fluorescence resonance energy transfer (FRET)-based probes.[33,34] Nonresponsive probes generated by the coexpression of a tagged fluorescent protein with pleckstrin homology (PH) domains of PIP3 binding proteins like Akt rely on diffusion-limited probe translocation to PIP3-rich regions.[24,37,38] These probes afford large background signals from the unbound probe and hence cannot be used to get conclusive information on PIP3 localization.

Engineered PH domains of proteins like Akt and GRP1 have also been used to develop FRET-based probes by leveraging PIP3 binding-induced structural changes and can afford information on PIP3 localization and PIP3 dynamics in the cell membrane.[33,40] However, FRET-based sensors often afford small-signal changes and low signal-to-noise ratios. A dimerization-dependent fluorescent protein-based sensor has also been used to develop a PIP3 sensor.[34] The probe utilizes the same engineered PH domain of Akt that was earlier used to develop a FRET-based sensor,[33] with an additional feature of single wavelength emission, allowing simultaneous imaging of PIP3 and PI(4,5)P2.[34] All genetically encoded probes, however, have to be introduced into cells via transient transfection. Transient transfection is a time-consuming technique compared to working with probes that might be able to enter cells via direct incubation in a few minutes.[41] Moreover, transfection often does not occur with similar efficiency in all cell types. Even within a single cell type, incorporation of plasmids encoding the probes can be nonuniform, leading to variability in results from one cell to another.[41] A hybrid protein−dye conjugated probe generated by attaching a polarity-sensitive dye to an engineered PH domain of myosin X protein has been utilized to image PIP3 in cells.[35,39] However, such modified protein-based probes have to be incorporated into cells via microinjection[35,39] and can only be used to image single cells one at a time.[41] Apart from tedious cell incorporation methods, all protein-based probes for PIP3 detection report slower time scales of PIP3 dynamics due to the diffusion-limited movement of these large probes within the cellular environment.[18,42−44] Finally, while few nonresponsive fluorescent protein-tagged probes can image nuclear PIP3 pools, no PIP3-responsive turn-on/ratiometric protein-based probe has been able to image the subnuclear localization of PIP3. All responsive probes are limited to studies of PIP3 pools in the plasma membrane.[34,37,39] Further, among the few nonresponsive PIP3 probes, most respond to both PIP3 and phosphatidylinositol-3,4-bisphosphate (PI(3,4)P2).[4] This poses a challenge for imaging the nuclear PIP3 pool since PI(3,4)P2 is also present within the nucleus.[27]

In this study, we have developed two short-peptide-based, environment-sensitive, ratiometric fluorescent sensors, **MFR-K17H** and **DAN-NG-H12G**, that rapidly enter the cell cytoplasm and orthogonally target and image the plasma membrane and nuclear PIP3 pools, respectively. **MFR-K17H** exhibited up to 45 times increase in visible fluorescence emission in the presence of 6.5 μM PIP3 with a limit of detection of 193 nM. The probe also afforded a significant 115 nm blue shift upon PIP3 binding, making it a ratiometric sensor. The sensor has been computationally designed based on analysis of molecular dynamics (MD) simulation results on a PI(4,5)P2 binding peptide, which had shown some affinity toward PIP3.[45] By scrutinizing the binding mode of the peptide with PI(4,5)P2 and PIP3 headgroups, the peptide was engineered rationally to flip lipid selectivity and generate the PIP3 sensor **MFR-K17H** (Figure 1). The sensor afforded selective emission response toward PIP3 over other physiologically relevant phospholipids, including other members of the phosphoinositide family of lipids to which PIP3 belongs. Along with significant and selective signal changes in the presence of PIP3, the sensor was completely water soluble and cell permeable, entering cells within 25 min of incubation, which allowed rapid imaging of PIP3 dynamics within the plasma membrane of living cells. Importantly, ratiometric imaging with **MFR-K17H** rapidly illuminated the inherently high PIP3 pools in the plasma membrane of breast cancer cells.

DAN-NG-H12G exhibited a highly selective ratiometric response with a 49 nm shift in emission wavelength upon binding PIP3 and a limit of detection of 98 nM. The salient feature of **DAN-NG-H12G** was its high binding affinity (100 nM) for PIP3, which was >10-fold higher over other phosphoinositides, including PI(4,5)P2 and PI(3,4)P2 and >30-fold higher over other anionic phospholipids. **DAN-NG-H12G** was designed based on the sequence alignment of a PIP3 binding peptide, W-NG 28−43, with the parent peptide scaffold used in **MFR-K17H** (Figure 1), which allowed us to fine-tune the W-NG 28−43 sequence and distinctly improve its selectivity toward PIP3. **DAN-NG-H12G** not only permeated the cell membrane but also permeated the nuclear membrane within <5 min incubation time as recorded via live time-lapse imaging. This sensor was also completely water-soluble, and ratiometric analysis of live cell images showed that the probe clearly marked nuclear PIP3 pools within the nuclear membrane and the nucleolus. Since **DAN-NG-H12G** was an environment-sensitive ratiometric probe, in a key result, we were able to reveal the organization of PIP3 within the nucleolus.

https://doi.org/10.1021/jacsau.3c00738
JACS Au 2024, 4, 1004−1017

RESULTS

Designing Cell-Permeable PIP3-Selective Sensors

To design cell-permeable sensors to detect PIP3 which is present in the inner leaflet of the plasma membrane and in the nucleus, the first requirement is a cell-permeable PIP3 binding molecular scaffold. Designing a small-molecule-based binding scaffold selective to the PIP3 headgroup (Figure S1) is extremely challenging due to its low abundance and the presence of seven structurally similar phosphoinositides in the cell membrane (Figure S1). The difficulty therefore lies in developing a binding scaffold that will detect PIP3 over other phosphoinositides along with other physiologically more abundant anionic phospholipids. We explored three strategies to design PIP3-selective cell-permeable binding scaffolds: (1) scanning PIP3 binding proteins with structurally characterized PIP3 binding sites in the search for PIP3 binding peptide sequences; (2) modifying structurally characterized peptide sequences with defined PI(4,5)P2 binding sites to generate PIP3 binding scaffolds; and (3) fine-tuning the selectivity of a PIP3 binding peptide with an undefined PIP3 binding site via comparison of its sequence and structural propensities with that of structurally characterized PI(4,5)P2 binding peptides.

The first strategy was to study the lipid-binding sites of PIP3 binding proteins and search for short ∼10 to 20 amino acid peptide sequences within these proteins that might bind to PIP3 and might also be cell permeable. Most PIP3 binding proteins bind to PIP3 via a PH domain.[1,45] PH domains bind to phosphoinositides through directional electrostatic interactions of positively charged amino acids with the negatively charged headgroup of a phosphoinositide. However, the positively charged amino acid residues in PH domains reside on different peptide strands. Chemically mimicking the phosphoinositide binding site of PH domains seemed nontrivial.

We therefore next investigated the binding sites of actin-regulatory proteins like Gelsolin, which have short peptide sequences that can bind to PI(4,5)P2,[46,47] a close structural analogue of PIP3. In a previous study, we had developed a cell-permeable PI(4,5)P2 sensor based on a 20 amino acid PI(4,5)P2 binding sequence from Gelsolin, Gel 150−169 (Figure 1(D)), which had a reported NMR structure.[48] In a separate study, we also investigated the structural propensities of the peptide in the presence of PI(4,5)P2 by performing MD simulations.[49] In brief, we generated a lipid bilayer membrane containing phosphatidylcholine (PC), which is a major phospholipid present in eukaryotic cell membranes (50% of total phospholipids)[50] and embedded a single PI(4,5)P2 lipid on one leaflet of the bilayer, following which we ran a simulation of the Gel 150−169 peptide in the presence of the membrane.[49] These simulations have been recently extended by us to develop second-generation improved PI(4,5)P2 sensors by performing additional simulations with other phosphoinositides, including PIP3, to understand the origin of selectivity of the Gel 150−169 peptide toward PI(4,5)P2 (see the SI for a brief overview of previous computational studies). The results from the MD simulations have been analyzed here from a new perspective in light of the goal of developing a PIP3 sensor.

Since PIP3 and PI(4,5)P2 are structurally similar, it is expected that a PI(4,5)P2 binding peptide would also bind to PIP3 with some affinity.[45,51] We decided to study the binding mode of the Gel 150−169 peptide with both lipids. Specifically, we asked the following question: is there any difference in the binding mode of the Gel 150−169 peptide toward PI(4,5)P2 versus PIP3 and can this difference be leveraged to flip the selectivity of the peptide toward PIP3? The results from the MD simulations indicated that positively charged amino acid residues near the C-terminus of the peptide formed stable salt bridge interactions with the negatively charged phosphate moieties of phosphoinositide headgroups (Figure 1(A−C)). In order to find out if there is any residue-wise difference in the interaction of the peptide with the two lipid headgroups, distances between the charged moiety on a positively charged amino acid and the different phosphate moieties on the lipid headgroups were calculated throughout the simulation runs. The calculations were performed for all positively charged amino acids present in Gel 150−169 (Figures 1(E−H) and S3). The results indicated that Arg 20 formed a stable electrostatic contact with the 5-phosphate group of PI(4,5)P2 (distance between charged residues was 4 Å or less) (Figure 1(E)). Lys 17 formed contacts with both 4- and 5-phosphate groups of PI(4,5)P2 (Figure 1(E,F)). On the other hand, Arg 19 formed stable electrostatic contacts with 4- and 5-phosphate groups of PIP3 (Figure 1(G,H)), while Arg 20 formed contact with the 4-phosphate group (Figure 1(H)). No residue came to within 4 Å of the 3-phosphate group of PIP3 (Figure S3(D)). Lys 17 did not form a stable contact with the PIP3 headgroup (Figure 1(G,H)), while Arg 19 did not form a stable contact with PI(4,5)P2 (Figure 1(E,F)). Based on this computational analysis, we hypothesized that if the directional contact of Lys 17 with the 4- and 5-phosphate groups of PI(4,5)P2 could be perturbed, the resultant peptide would lose its affinity toward PI(4,5)P2 and might show preferential selectivity toward PIP3.

A novel mutant peptide, K17H, was therefore designed by replacing Lys 17 with a histidine, which is also a positively charged amino acid, in order to maintain the charge of the peptide (Figure 1(I)). We reasoned that the histidine residue would affect the directional electrostatic interaction between the 17th amino acid residue of the peptide and the 4- and 5-phosphate groups of PI(4,5)P2 without affecting the cell permeability of the peptide, which is possibly related to its overall positive charge. A second mutant peptide, R20H, in which Arg 20 was replaced with a histidine, was also designed as a control (Figure 1(J)). Since the computational studies predicted that Arg 20 interacted with at least one phosphate group on both lipid headgroups, we expected that replacing this amino acid would reduce the binding affinities of the peptide toward both lipids.

MD simulations on the Gel 150−169 peptide had shown that the N-terminal half of the peptide interacted with the hydrophobic part of the membrane after electrostatic contacts were established between the C-terminus of the peptide and the negatively charged phosphoinositide headgroup.[49] Based on this information, we attached a polarity-sensitive dye[52] to the N-terminus of the K17H and R20H peptides to convert them into lipid responsive sensors (Figure 1(I,J)). The resultant molecules were expected to afford a shift in emission wavelength upon binding to a specific phosphoinositide due to a change in the polarity when the N-termini of the peptides interacted with the membrane. Two probes, **MFR-K17H** and **MFR-R20H**, were synthesized by conjugating a carboxylic acid derivative of a polarity-sensitive fluorene dye (MFR dye, Figures S4 and S5) with the N-terminus amine groups of the peptides.

In the final strategy, we explored a PIP3-selective synthetic peptide, W-NG 28−43, derived from a Calmodulin-binding protein Neurogranin.[53] The exact PIP3 binding site in W-NG 28−43 is not known, and its structure remains uncharacter-

https://doi.org/10.1021/jacsau.3c00738
JACS Au 2024, 4, 1004−1017

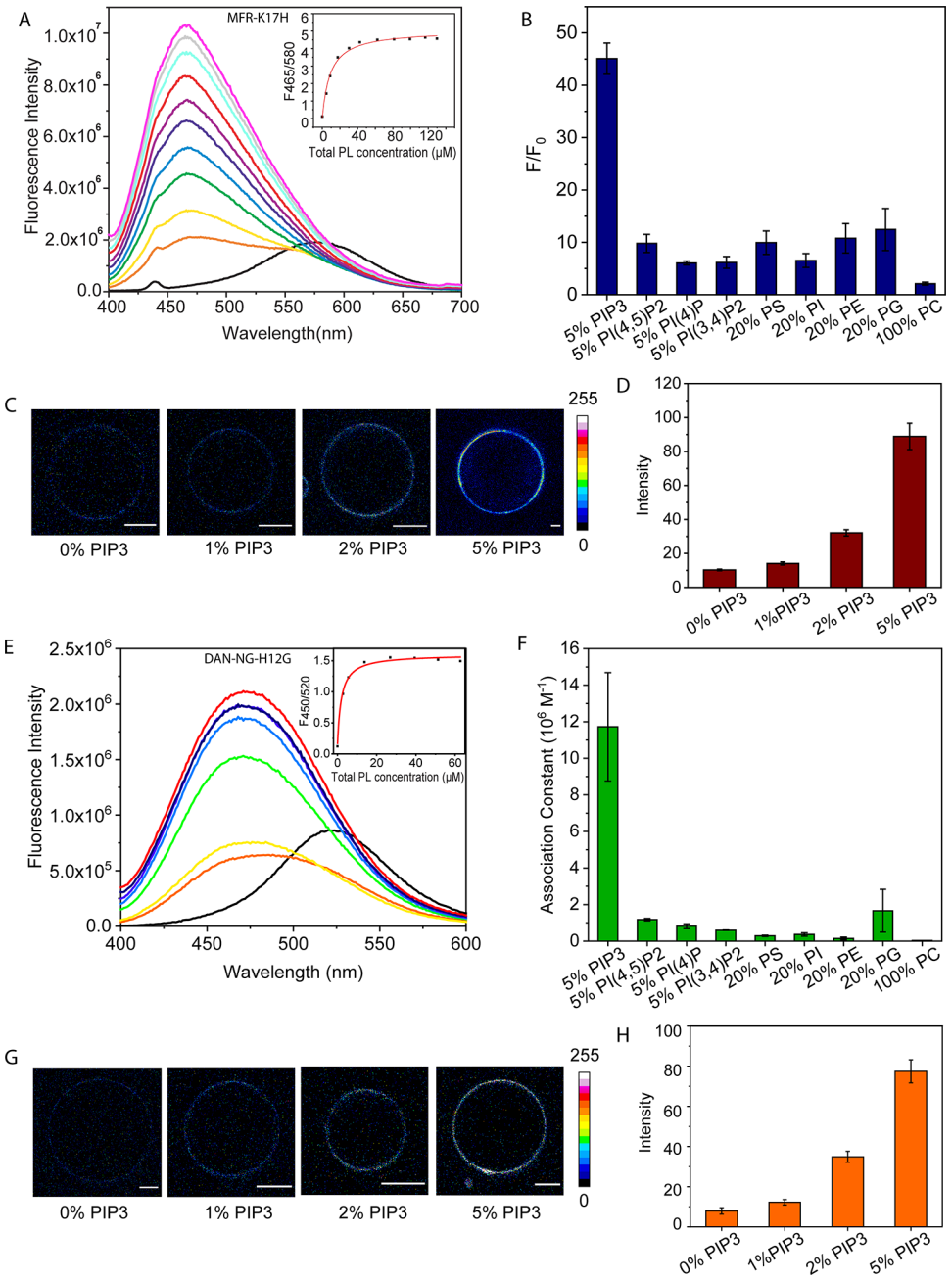

Figure 2. In vitro selectivity and sensitivity of **MFR-K17H** and **DAN-NG-H12G**. (A) Fluorescence response of **MFR-K17H** (1 μM) with increasing levels of 5% PIP3-PC mixed vesicles. **MFR-K17H** (black) and total phospholipid concentrations of 5% PIP3 SUVs: 4.4 μM (orange), 8.8 μM (yellow), 17.5 μM (green), 30.2 μM (indigo), 42.6 μM (blue), 62.4 μM (purple), 81.3 μM (red), 99.4 μM (cyan), 116.6 μM (gray), and 130 μM (magenta). Inset: The plot of the emission intensity ratio of 465 and 580 nm versus the concentration of the total phospholipid. (B) Comparison of "turn-on" response of **MFR-K17H** toward phosphoinositides and other physiologically relevant phospholipids. (C) Confocal fluorescence images showing the response of **MFR-K17H** (500 nM) in GUVs with different PIP3 levels. (D) Bar plots representing the average intensities along the perimeter of the GUVs. (E) Fluorescence response of **DAN-NG-H12G** (1 μM) with increasing levels of 5% PIP3-PC mixed vesicles. **DAN-NG-H12G** (black) and total phospholipid concentrations of 5% PIP3 SUVs: 2.5 μM (orange), 5.6 μM (yellow), 13.7 μM (green), 26.8 μM (indigo), 39.3 μM (blue), 51.3 μM (purple), and 62.6 μM (red). Inset: The plot of the emission intensity ratio of 450 and 520 nm versus the concentration of the total phospholipid. The plot was fitted to calculate the dissociation constant (K_d) of **DAN-NG-H12G** toward 5% PIP3-PC vesicles. (F) Bar plots representing the association constant values of **DAN-NG-H12G** obtained for different phospholipids. (G) Confocal fluorescence images showing the response of **DAN-NG-H12G** (1 μM) in GUVs with different PIP3 levels. (H) Bar plots representing the average intensities along the perimeter of the GUVs. All bar plots are presented as the mean ± SEM, where N = 3. Scale bar: 10 μm.

ized.[54] In fact, based on the presence of several positively charged basic residues in the C-terminus of this peptide and hydrophobic residues in its N-terminus, it was speculated that its mode of interaction with phosphoinositides would be similar to peptides derived from PI(4,5)P2 binding actin-regulatory proteins like Gelsolin and Villin.[53] Both the electrostatic and hydrophobic interactions seemed necessary for the binding of W-NG 28−43 to PIP3.[53] In the absence of any reported structure of the W-NG 28−43 peptide, MD simulations were nontrivial. Hence, we aligned the sequence of W-NG 28−43

https://doi.org/10.1021/jacsau.3c00738
JACS Au 2024, 4, 1004−1017

with that of Gel 150−169 and noted that Lys 17 in Gel 150−169 aligned with His 12 in W-NG 28−43 (Figure 1(K)). We hypothesized that if the binding modes of Gel 150−169 and W-NG 28−43 to phosphoinositides were indeed similar, a mutation at this site would significantly improve the PIP3 to PI(4,5)P2 selectivity of this peptide, affording a highly PIP3-selective probe. To perform a quick check on whether this hypothesis would work, we leveraged tryptophan, a polarity-sensitive amino acid, that happened to be fortuitously present in the N-terminus of the peptide. We synthesized W-NG 28−43 and a novel mutant peptide W-NG-H12G (Figure S6). For W-NG 28−43, the parent peptide, we observed a ∼35 nm blue shift in the emission maxima of tryptophan in the presence of increasing levels of PIP3 compared to a ∼12 nm blue shift in the emission maxima of tryptophan in the presence of increasing levels of PI(4,5)P2 (Figure S7). On the other hand, for W-NG-H12G, the mutant peptide that we designed, we observed a ∼43 nm blue shift in the emission maxima of tryptophan in the presence of increasing levels of PIP3 and barely a ∼7 nm blue shift in the emission maxima of tryptophan in the presence of increasing levels of PI(4,5)P2 (Figure S7). This data implied that W-NG-H12G had a greater selectivity toward PIP3 over PI(4,5)P2 than the parent peptide. We therefore proceeded to use the new W-NG-H12G peptide that we designed to develop a PIP3-selective sensor. Since the excitation of tryptophan at 290 nm was not appropriate for live cell imaging and, importantly, there would be background from endogenous tryptophan within cells, we attached a polarity-sensitive dansyl (DAN) (Figure S8)-based dye to the N-terminus of the peptide by replacing tryptophan with a cysteine residue in order to develop the novel PIP3 probe. The choice of the dye was based on its size, which was similar to that of tryptophan. **DAN-NG-H12G** was hence synthesized by conjugating acrylodan to the cysteine thiol moiety (Figures 1(L), and S8, and S9).

All three synthesized probes, **MFR-K17H**, **MFR-R20H**, and **DAN-NG-H12G**, were water soluble; hence, all experiments were performed in an aqueous buffer without the addition of any organic solvent.

MFR-K17H and DAN-NG-H12G are PIP3-Selective Ratiometric Fluorescent Sensors

The **MFR-K17H** and **DAN-NG-H12G** molecules were first tested for their fluorescence response toward different physiologically relevant phospholipids in an aqueous buffer by using small-unilamellar vesicles (SUVs) of phospholipids (details of SUV composition are given in the SI). When excited at 390 nm, **MFR-K17H** exhibited an emission spectrum with a maxima at 580 nm (Figure 2(A)). Upon adding increasing levels of 5% PIP3-PC vesicles, the emission spectrum showed a maximum 115 nm blue shift at saturation. This afforded a spectrum with a peak at 465 nm. The emission intensity of the peak at 465 nm increased with increasing levels of 5% PIP3-PC vesicles (Figure 2(A)). A maximum of 45 times enhancement was observed at 465 nm at saturating levels of PIP3, 6.5 μM (130 μM total phospholipid) (Figure 2(B)). Importantly, the "turn-on"-response of **MFR-K17H** was the highest for PIP3 when compared to other physiologically relevant phospholipids. Hence, **MFR-K17H** responded to PIP3 both in a ratiometric manner with a shift in emission wavelength and in a "turn-on" mode with a significant PIP3-selective emission enhancement. The "turn-on" response data of the probe was used to determine the limit of detection (LOD) of the probe for PIP3 sensing. The LOD was 193 nM, which is on the lower side of expected PIP3 levels in cellular systems. The quantum yields for **MFR-K17H** and PIP3-bound **MFR-K17H** were determined to be 0.33 and 0.89, respectively (Figure S10). **DAN-NG-H12G** was excited at 380 nm and exhibited an emission peak at 520 nm (Figure 2(E)). Upon adding increasing levels of 5% PIP3-PC vesicles, the emission spectrum showed a maximum 49 nm blue shift at saturation. This afforded a spectrum with a peak at 471 nm. The emission intensity of the peak at 471 nm increased with increasing levels of 5% PIP3-PC vesicles (Figure 2(E)). The quantum yields for **DAN-NG-H12G** and PIP3-bound **DAN-NG-H12G** were determined to be 0.21 and 0.59, respectively (Figure S10). The LOD for the **DAN-NG-H12G** probe was calculated to be 98 nM and was very close to the expected overall cellular concentrations of PIP3.

We next determined the binding affinities of the **MFR-K17H** and **DAN-NG-H12G** probes with different phospholipids by fitting either the fluorescence intensity at the maxima of the lipid-bound form (465 nm) or the ratio of blue to green emissions with increasing lipid concentrations, to a 1:1 binding model detailed in SI section 4 (Figure 2(A,E, inset)). The dissociation constant of the **MFR-K17H** probe toward PIP3 was 1.4 ± 0.1 μM and that of **DAN-NG-H12G** was 14-fold lower at 100 ± 50 nM (Table S2). We observed that the binding constants for each sensor were similar when dissociation constants were calculated from titrations with either 5% PIP3-PC vesicles or 2% PIP3-PC vesicles (Figure S11), indicating that the binding of the sensors to PIP3 was specific. Further, adding another anionic phospholipid in the vesicles (5% PIP3, 20% PG, 75% PC) did not alter the dissociation constants of the sensors toward PIP3, thus validating the binding specificity of the sensors toward PIP3 (Figures S12 and S13). The dissociation constant for the **MFR-K17H** probe toward PIP3 was the lowest when compared to that of other physiologically relevant phospholipids titrated as vesicles containing 5% phosphoinositides in PC, 20% other abundant anionic phospholipids in PC, and 100% PC (Table S2). The **DAN-NG-H12G** probe showed a ∼10 times higher affinity for PIP3 over PI(4,5)P2 (Figure 2(F)). A ∼13 times lower affinity was observed for other phosphoinositides, including PI4P and PI(3,4)P2, and the rest of the lipids afforded $a > 30$ times lower affinity when compared to PIP3 (Table S2). Hence, **DAN-NG-H12G** was a highly selective, high-affinity, sensitive, ratiometric PIP3 sensor.

As expected, the control probe **MFR-R20H** afforded lower binding affinities toward both PI(4,5)P2 and PIP3 (Table S2). As predicted via computational analysis, the K17H peptide had an enhanced affinity toward PIP3 when compared to the R20H mutant. Importantly, when **MFR-K17H** and **DAN-NG-H12G** were applied in a fluorescence confocal microscopy setup (λ_{ex} 405 nm) to image increasing levels of PIP3 in giant unilamellar vesicles (GUVs), vesicles containing as low as 1% PIP3 in PC could be visualized (Figure 2(C,G)). Intensity analysis of the GUV images indicated that both probes could effectively report on increasing levels of PIP3 in a confocal microscopy setup (Figure 2(D,H)). Hence, by utilizing insights from molecular dynamics simulations and peptide sequence correlations, we developed two peptide-based ratiometric PIP3-selective probes. Next, we proceeded to test the in-cell response and the in-cell specificity of the probes toward PIP3 imaging.

https://doi.org/10.1021/jacsau.3c00738
JACS Au 2024, 4, 1004−1017

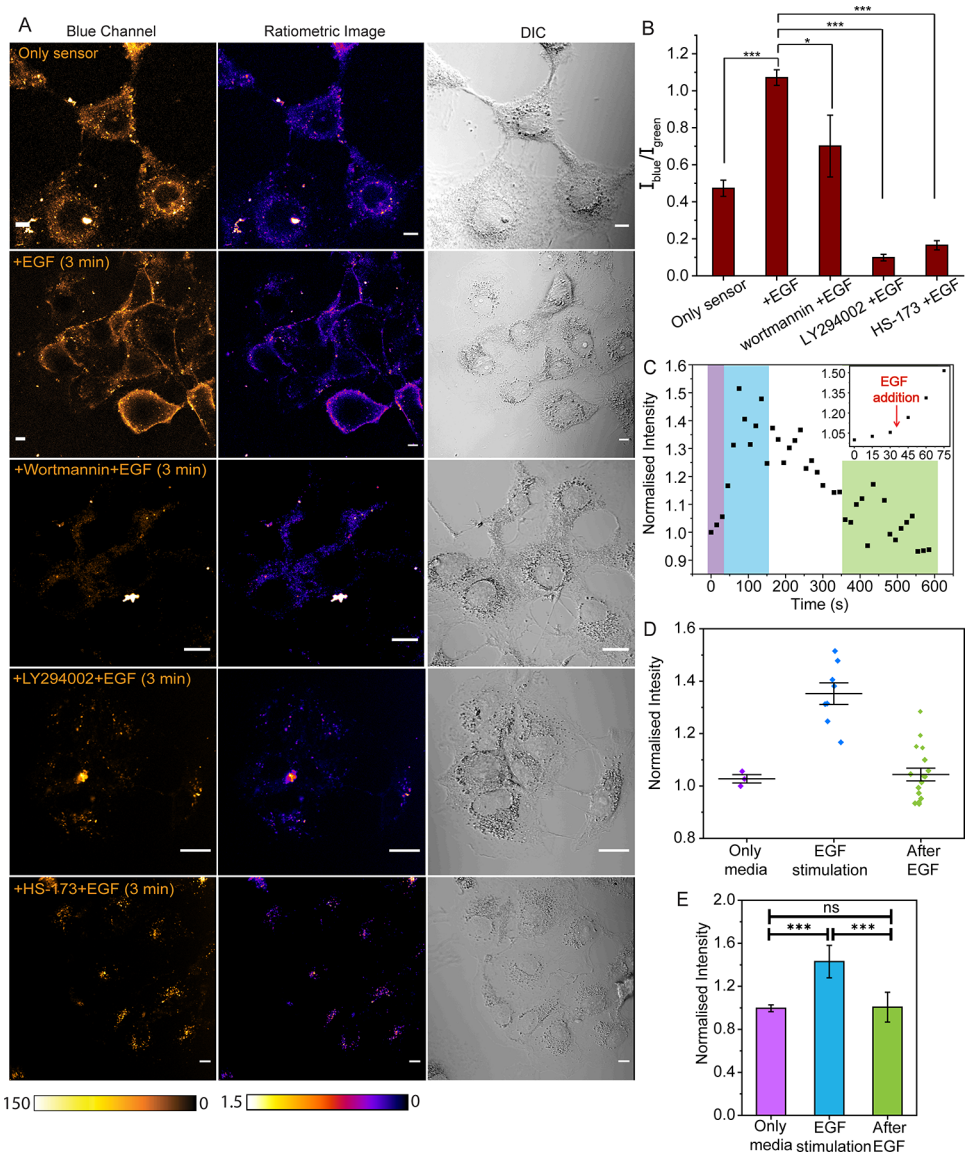

Figure 3. Imaging growth factor-induced PIP3 dynamics in living COS-7 cells with cell-permeable PIP3 sensor **MFR-K17H**. All cells were directly incubated with **MFR-K17H** (5 μM) for 20−25 min at 37 °C in serum-free DMEM media. (A) First column, confocal images (λ_{em}: 425−510 nm) of living COS-7 cells treated with **MFR-K17H** (5 μM): without external stimuli (first row), with EGF for 3 min (second row), wortmannin (0.5 μM) followed by EGF for 3 min (third row), LY294002 (50 μM) followed by EGF for 3 min (fourth row), and HS-173 (1 μM) followed by EGF for 3 min (last row). The second column represents the ratiometric images, and the third column represents the differential interference contrast (DIC) images for the same cells displayed in the first column. Scale bar: 10 μm. (B) Ratiometric fluorescence intensity bar plot representing average plasma membrane intensity ($N = 3$) values for only sensor, after EGF stimulation, and PI3K inhibitor-treated cells upon EGF stimulations. (C) Representative real-time tracking of fluorescence intensities of **MFR-K17H** on the plasma membrane of COS-7 cells following EGF stimulation (λ_{ex} = 405 nm, λ_{em}: 425−510 nm). Time points are marked by color shades: before the addition of EGF (purple), after EGF addition (blue), and after the decrease of the sensor signal to basal levels (green). Inset: Zoomed-in representation of 0−80 s time scale was used to show the sharp increase in sensor intensity after EGF addition (at 30 s). (D) The representative scatter plot of intensities from the plasma membrane during three events highlighted in (C) in a real-time tracking experiment with mean emission intensities. (E) The normalized fluorescence intensity bar plot representing average plasma membrane intensity values for only media, after EGF addition, and after a decrease of the sensor signal to basal levels for time slots indicated by different colors in (C). Data presented as mean ± s.d, where $n \geq 6$ for each set ($N = 3$). Statistical analyses were performed on 3 independent sets of experiments using an unpaired, two-tailed student's *t*-test. *$p < 0.05$; **$p < 0.01$; and ***$p < 0.001$.

Cell-Permeable PIP3 Sensor, MFR-K17H, Tracks Epidermal Growth Factor-Induced Rapid PIP3 Enhancement in the Plasma Membrane, Live

Cell-permeable PIP3 sensors are required because PIP3 is present in the inner side of the cell membrane and within the nucleus. A major drawback of all existing PIP3 sensors is cell impermeability. We first tested whether **MFR-K17H** was cell permeable. Living cells directly incubated with the sensor for 20−25 min were imaged on a confocal fluorescence microscopy setup, and emission was collected both in the blue (425−510 nm) and green (520−600 nm) emission channels (Figure S14(A)). The intensity in the green channel represented emission from both bound and unbound sensors (Figures 2(A) and S29), while the intensity in the blue channel majorly represented emission from the bound sensor, although there was minimal overlap with the tail of the unbound probe emission

https://doi.org/10.1021/jacsau.3c00738
JACS Au 2024, 4, 1004−1017

(Figures 2(A) and S29(A)). We observed emission in both the blue and green channels from the cytoplasm of cells incubated with the probe, which did not colocalize with any specific organelle tracker (Figure S15). Cell images from different z-planes showed the clear incorporation of the probe in living cells (Figure S14(B)). From this experiment, we could distinctly confirm that the **MFR-K17H** probe entered living cells within 20−25 min of direct incubation (Figure S14). Importantly, we noted that in resting, unstimulated living cells, there was very low fluorescence intensity of the bound **MFR-K17H** probe (blue channel) from the cell membrane (Figure 3A, top, left panel), leading to a low-intensity ratio of blue to green emission intensity (Figure 3B). This observation is consistent with the fact that PIP3 levels are very low in resting cell membranes. This data also indicated that the sensor was not detecting other anionic lipids that were constitutively present in the cell membrane, including PI(4,5)P2, which is structurally the closest to PIP3. The **MFR-K17H** probe did not show any emission from the nucleus. Probe uptake was lower at 4 °C, hinting at an active transport pathway for the probe (Figure S16). **MFR-K17H** was not toxic to cells up to the tested concentration of 10 μM (94% cell viability for COS-7 cells), which is higher than the concentration that was used for all cell studies (Figure S17). Overall, the data show that **MFR-K17H** is a cell-permeable, fluorescent PIP3 sensor. We next proceeded to test the applicability of the probe toward selective imaging of PIP3 dynamics in living cells and validate the in-cell PIP3 selectivity of **MFR-K17H**.

An early step of cell proliferation and cell growth signaling is the production of PIP3, which occurs upon the activation of receptor tyrosine kinases like the epidermal growth factor receptor (EGFR).[14,55] Binding of the epidermal growth factor (EGF) to EGFR leads to the activation of PI3K, which converts PI(4,5)P2 to PIP3 and triggers downstream growth signaling pathways.[15,55−57] Understandably, overexpression of EGFR and dysregulation of the EGFR-PI3K-Akt pathway leads to increased PIP3 levels and is associated with many cancers, especially malignant forms.[22,55,58] With this background, in order to test whether the cell-permeable probe **MFR-K17H** could track PIP3 dynamics in living cells, we selected COS-7 cells, which endogenously express ∼10^5 EGFR copies per cell[59] and are frequently employed to study EGFR activation.[60] First, we tested the photostability of the **MFR-K17H** sensor by incubating COS-7 cells with the probe and irradiating the cells at the same region-of-interest at 30 s intervals with a 405 nm laser in a confocal microscopy setup for ∼10 min (Figure S18). The imaging time was selected to be 10 min based on previous studies on the kinetics of PIP3 production in EGF-stimulated cells.[34,35] The probe emission intensity for both blue and green imaging channels and hence the ratio remained unchanged, indicating that **MFR-K17H** was photostable and could be taken forward for imaging PIP3 dynamics in living cells.

Next, the effect of EGF stimulation on COS-7 cells incubated with the **MFR-K17H** sensor was studied in a confocal microscopy setup to investigate whether the sensor could report on PIP3 dynamics in living cells. EGF addition led to a distinct signal increase in the blue channel emission and a concomitant increase in the ratio of blue to green emission of **MFR-K17H** at the plasma membrane (Figure 3(A), second row, and 3(B)). A similar plasma membrane signal enhancement was also observed upon EGF addition to cells transfected with **PH-Akt-GFP**, which is a protein-based PIP3 sensor (Figure S19(B)). In the case of **PH-Akt-GFP**, however, the background emission from the cytoplasm was much higher (Figures S19 and S20). Hence, the relative membrane signal to cytoplasm background ratio was significantly enhanced in the case of **MFR-K17H** (Figure S20). The result indicated that **MFR-K17H** could report on PIP3 dynamics in living cells and afforded ratiometric imaging along with distinctly lower background signals compared to an existing frequently employed protein-based probe (Figures 3(A) and S19). Further, when the cell imaging data were compared for **PH-Akt-GFP** and **MFR-K17H**, it was observed that while **MFR-K17H** could enter all cells within a plate via direct incubation, expression of **PH-Akt-GFP** varied from cell to cell (Figure S21). This data highlighted another key advantage of our cell-permeable probe.

To conclusively confirm that **MFR-K17H** was indeed detecting PIP3 in living cells, three PI3K inhibitors, Wortmannin, HS-173, and LY294002, were employed. Among these three inhibitors, HS-173 is exclusively selective toward PI3K. LY294002 is a potent PI3K inhibitor. Wortmannin can also inhibit a few other phosphatidylinositol kinases, albeit only at higher μM concentrations.[61] Since PI3K is the enzyme that synthesizes PIP3 in cell membranes, selective and potent inhibitors such as HS-173 and LY294002, respectively, would completely abolish PIP3 synthesis from the cell membrane. Indeed, cells treated with PI3K inhibitors[62,63] showed a significantly reduced ratiometric signal in the plasma membrane upon EGF stimulation compared to cells untreated with inhibitors (Figure 3(A,B)). This data distinctly showed that **MFR-K17H** could detect intracellular PIP3 with exquisite specificity and selectivity (Figure 3(B)).

Analysis of time-lapse imaging (Video 1) of COS-7 cells stimulated with EGF showed a rapid increase in membrane intensity of the probe in the blue channel within 45−60 s of EGF addition (Figure 3(C, inset)), which remained high until ∼75 to 120 s post addition (Figure 3(C−E)). Following that, the signal in the membrane decreased and returned to basal levels within ∼4 to 6 min post EGF addition (Figure 3(C−E)). Importantly, as per the photostability data, the probe was photostable within the time range of the experiment (Figure S18), and cells untreated with EGF did not show any enhancement in the probe emission at the cell membrane (Figure S22). A maximum 60% enhancement in the emission intensity of **MFR-K17H** was observed in the plasma membrane of the COS-7 cells upon EGF stimulation. Hence, **MFR-K17H** is a cell-permeable, visible-excitable, ratiometric fluorescent sensor that can selectively track PIP3 dynamics in living cells.

It is imperative here to compare the response of **MFR-K17H** with that of previously reported protein-based sensors (Table S1). Both Anti-PIP3 antibody staining of EGF-stimulated carcinoma cells[42] and ^{32}P labeling studies in growth factor-stimulated fibroblasts[44] had shown fast PIP3 kinetics (PIP3 levels peaking at <1 min) compared to studies using protein-based probes.[34,39] Specifically, PIP3 levels in the plasma membrane were highest at ∼1 min after EGF stimulation when PIP3 was detected using antibody staining and at 40 s for ^{32}P labeling studies.[42,44] For the antibody method, the staining remained detectable until 3 min post stimulation and came down to basal levels within 4−5 min of stimulation.[42] In the same study, a GFP-tagged PH domain showed a rise in PIP3 levels, but the intensity did not come down to basal levels even after 5 min post stimulation.[42] Based on these results, the authors concluded that PH domain-based probes interfered with the binding of proteins necessary for the depletion of PIP3 from the membrane, which is an integral part of PIP3 dynamics.[42] The

https://doi.org/10.1021/jacsau.3c00738
JACS Au 2024, 4, 1004−1017

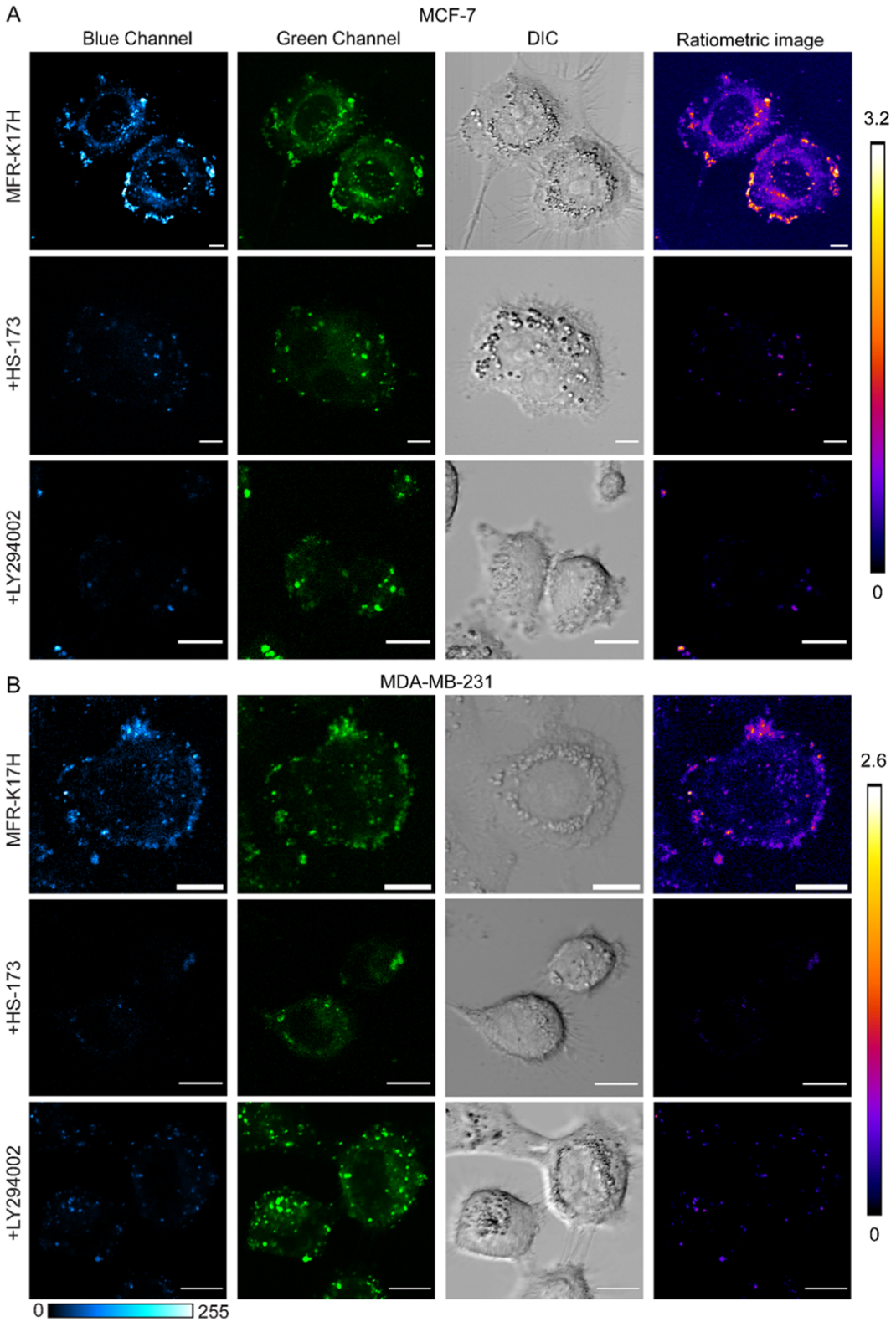

Figure 4. Ratiometric Imaging of PIP3 in breast cancer cell lines. Both the breast cancer cell lines, MCF-7 and MDA-MB-231 cells, were incubated with **MFR-K17H** (5 μM) for 25 min at 37 °C in imaging media. (A) Confocal images of living MCF-7 cells treated with **MFR-K17H**: without PI3K inhibitors (first row), with the application of potent PI3K inhibitors, HS-173 (second row) and LY294002 (third row), respectively. (B) Confocal images of living MDA-MB-231 cells treated with **MFR-K17H** (5 μM): without PI3K inhibitors (first row), with the application of PI3K inhibitors, HS-173 (second row) and LY294002 (third row), respectively. Scale bar, 10 μm. The images are representative of at least three biological replicates from different cell plates.

response of **MFR-K17H** in EGF-stimulated cells peaked at <1 min post EGF addition, remained detectable until 2−3 min, and completely decayed by 4−6 min, which mirrored the PIP3 dynamics time scales that were previously reported using an anti-

https://doi.org/10.1021/jacsau.3c00738
JACS Au 2024, 4, 1004−1017

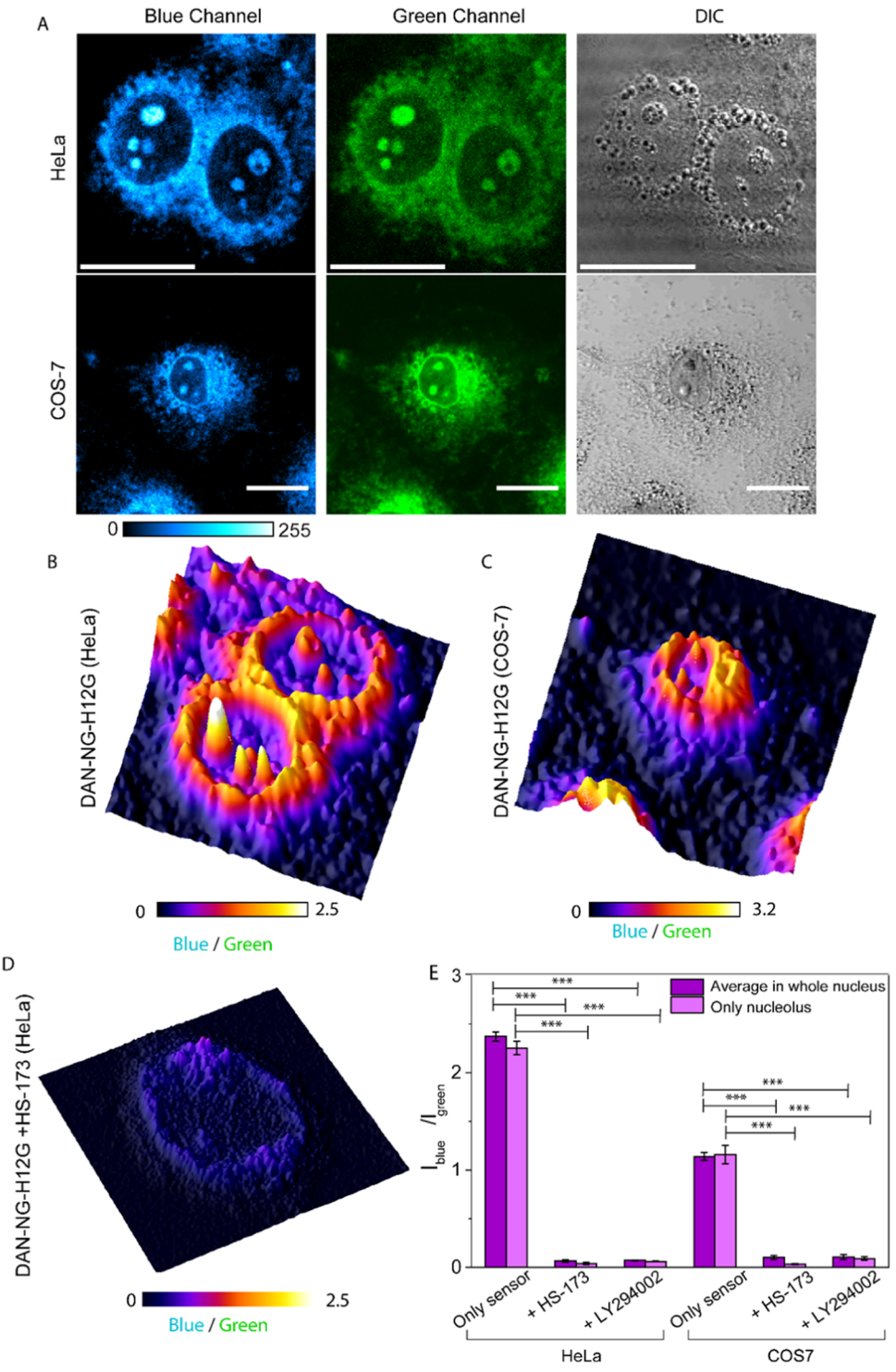

Figure 5. Imaging nuclear PIP3 pools with **DAN-NG-H12G** in HeLa and COS-7 cells. All cell types were directly incubated with **DAN-NG-H12G** (5 μM) at 37 °C in serum-free DMEM media for 5 min. (A) Representative confocal single z-plane images of living HeLa cells (first row) and COS-7 cells (second row), showing nuclear PIP3 pools illuminated by **DAN-NG-H12G**. λ_{ex} 405 nm laser. Fluorescence emission: blue channel (λ_{em}: 435−465 nm); green channel (λ_{em}: 560−590 nm). Scale bar: 20 μm. (B, C) 3D intensity-based plots of ratiometric images of the above cells Hela and COS-7, respectively, generated from the blue/green ratio. The images are representative of at least three biological replicates from different cell plates. (D) 3D intensity-based plots of ratiometric image of HS-173 (1 μM)-treated HeLa cells. (E) The ratiometric fluorescence intensity bar plot representing the average **DAN-NG-H12G** intensity ratio in nucleus and nucleolus for only the sensor and after the addition of potent PI3K inhibitors, HS-173 and LY294002 in HeLa and COS-7 cells, where $n \geq 8$ for each set ($N = 3$). Statistical analyses were done on 3 independent sets of experiments using an unpaired, two-tailed student's *t*-test. *$p < 0.05$; **$p < 0.01$; and ***$p < 0.001$.

PIP3 antibody for the entire sequence and ^{32}P labeling studies for the PIP3 generation time scales.[42,44] On the other hand, a protein-based genetically encoded PIP3-responsive probe applied to the COS-7 cell line under the same experimental conditions as in our study showed a significantly slower rise in PIP3 levels which peaked only at 5 min post stimulation and did

https://doi.org/10.1021/jacsau.3c00738
JACS Au 2024, 4, 1004−1017

not decay to basal levels even after 15 min post stimulation.[34] Further, a PH domain-based responsive microinjectable probe showed a slow rise, peaking at ∼4 to 5 min and decaying to basal levels at 20 min post stimulation.[39] These comparisons point to a significant advantage of **MFR-K17H** in its ability to report fast PIP3 dynamics, which protein-based probes are not able to afford. Importantly, since **MFR-K17H** is a small-molecule-based, cell-permeable, responsive probe, it can report on PIP3 dynamics accurately in living cells without the requirement of cell fixing, which has also been reported to affect PIP3 localization.

MFR-K17H can Detect Endogenous PIP3 in Breast Cancer Cells

Since **MFR-K17H** is a cell-permeable PIP3-sensitive probe, it has the potential to be developed as a diagnostic agent for malignant cancers, especially breast cancer that is characterized by inherently higher levels of PIP3.[23] Chemo-resistant and malignant breast cancers are characterized by hyperactivating mutations in PI3K and dysfunctional PTEN mutants that lead to higher PIP3 levels and hence enhanced cell proliferation.[19,23] In order to test the future applicability of **MFR-K17H** toward cancer diagnostics, we explored PIP3 imaging in live breast cancer model cells MCF-7 and MDA-MB-231, the latter being a triple-negative breast cancer cell line. **MFR-K17H** permeated both cell lines within 20−25 min of incubation and distinctly highlighted the cell membrane without the requirement of any external chemical stimulation (Figure 4). Importantly, ratiometric analysis of the images indicated distinctly high blue to green emission ratios in the cell membranes of both breast cancer model cells (Figure S23). The bound channel (blue) emission of the **MFR-K17H** sensor colocalized with a membrane marker, indicating that the observed sensor emission was from cell-membrane PIP3 (Figure S24). This experiment once again validated the in-cell PIP3 specificity of **MFR-K17H**.

To ensure that the increased blue/green emission intensity ratio observed in cancer cell membranes was due to the selective binding of the probe to PIP3, we treated both cell lines with the potent PI3K inhibitors HS-173 and LY294002. Complete abolishment of the bound blue channel emission from cell membranes was observed (Figure 4(A) mid and bottom; 4(B) mid and bottom panels). Importantly, quantitative ratiometric image analysis (Figure S23) showed a significant decrease in the blue/green emission intensities from cell membranes of both the cancer cell lines when treated with the inhibitors compared to untreated cells. Therefore, the ability of the novel PIP3 probe **MFR-K17H** to rapidly and directly enter breast cancer cells and selectively image enhanced PIP3 levels opens an unprecedented path into future rapid breast cancer diagnostics along with a distinct possibility of fast identification of cancer cells that will respond to PI3K inhibitor therapy. This key scope is unavailable in current protein-based PIP3 probes that rely on either microinjection or transient transfection for cellular incorporation.

DAN-NG-H12G is a Cell-Permeable Ratiometric PIP3-Selective Probe that Images Nuclear PIP3 Pools

Following the studies with **MFR-K17H**, we next tested the cell permeability of the **DAN-NG-H12G** probe, which has a significantly higher affinity toward PIP3. Interestingly, we observed that the probe not only entered living cells, including COS-7 and HeLa cells, but also rapidly lit up the cell nucleus, based on live cell imaging experiments in a confocal fluorescence microscopy setup (Video 2, Figure S25, z-stack images). The emission was collected in both the blue (435−465 nm) and green (560−690 nm) emission channels (Figure 5(A)). The intensity in the green channel represented emission from both bound and unbound sensors, while the intensity in the blue channel majorly represented emission from the bound sensor, although there was minimal overlap with the tail of the unbound probe emission (Figures 2(E) and S29). We observed emission in both the blue and green channels from the nuclear region of cells incubated with the probe (Figure 5(A)). For all further image analysis and quantifications, we therefore relied on the ratio of blue to green channel emission intensities rather than absolute intensity in any particular channel. **DAN-NG-H12G** was not toxic to cells up to the tested concentration of 10 μM (96% cell viability for COS-7 cells), which was higher than the concentration that was used for all cell studies (Figure S26).

The intracellular staining of **DAN-NG-H12G** was very similar to that of anti-PIP3 antibody staining, with both **DAN-NG-H12G** and antibody staining lighting up perinuclear and nuclear regions, specifically the nucleoli (Figure S27). Previous studies with anti-PIP3 antibodies indicate the clear presence of PIP3 pools in the nucleolus (Figure S27), while PI(4,5)P2 and PI(3,4)P2 exist in nuclear speckles.[27] We only observed the lighting up of the nucleolus inside the nucleus with our probe and no nuclear speckles, indicating the high PIP3 specificity of the **DAN-NG-H12G** probe and, importantly, its distinct ability to light up the nucleolar PIP3 pools as shown by the ratiometric images Figure 5(B),5(C). This data indicated that the highly PIP3-specific **DAN-NG-H12G** probe targeted the intranuclear PIP3 pool.

To further confirm that the bound probe emission in the blue channel observed within the nucleus, specifically the nucleolus, was indeed due to the selective imaging of PIP3 by the **DAN-NG-H12G** probe, we set up an experiment to selectively deplete nuclear PIP3 pools. Since PI3K is responsible for PIP3 synthesis within the nucleus,[5] PI3K inhibitors, HS-173 and LY294002, were used. Upon treatment of living cells with PI3K inhibitors, we observed a complete reduction of bound probe signal (blue channel) from nucleoli (Figures 5(D) and S28) and a significant decrease in the ratio of blue to green emission of the probe (Figures 5(E) and S28) as quantified by ratiometric analysis, thereby conclusively validating the in-cell PIP3 selectivity of the **DAN-NG-H12G** probe. The decrease in the probe emission ratio in the nucleolus was also clearly reflected in the decrease in the average ratio within the nucleus (Figure 5(E)). To the best of our knowledge, this is the first ratiometric, cell-permeable fluorescent probe that can image the nuclear PIP3 pool.

Since the discovery of nuclear phosphoinositide pools, the organization of these lipids in membraneless structures has remained an open question.[27,31] While it was speculated that phosphoinositides would reside within such structures in an orientation that shields the fatty acid tails from the aqueous environment, there was no direct evidence.[27] As **DAN-NG-H12G** is a polarity-sensitive ratiometric PIP3 sensor, our imaging data showing high blue/green emission intensity ratios (Figure 5(B,C)) in the nucleolus also hint toward the fact that the nonpolar fatty acid tails of PIP3 reside in a hydrophobic region while the polar headgroup is still accessible to the aqueous environment for protein binding in membraneless structures like the nucleolus.

DISCUSSION AND CONCLUSIONS

We report two ratiometric fluorescent cell-permeable PIP3-selective probes: **MFR-K17H** and **DAN-NG-H12G**. **MFR-**

https://doi.org/10.1021/jacsau.3c00738
JACS Au 2024, 4, 1004−1017

K17H was designed based on MD simulation-guided modifications on a structurally characterized PI(4,5)P2 binding peptide. **DAN-NG-H12G** was designed by applying insights from the design of **MFR-K17H** to a structurally uncharacterized PIP3 binding synthetic peptide. Although we had not designed any specific intracellular targetability into our probe design, we serendipitously observed a remarkable orthogonal targetability of the two probes. **MFR-K17H** lit up cell-membrane PIP3 pools. **DAN-NG-H12G**, on the other hand, distinctly entered living cells within less than 5 min incubation times and lit up the nuclear PIP3 pools. Both sensors were ratiometric, and their in-cell PIP3-selective responses were distinctly abolished in the presence of highly selective inhibitors of the enzyme PI3K that is responsible for PIP3 synthesis, conclusively validating their in-cell PIP3 selectivity. **MFR-K17H** could be applied to track rapid <1 min growth factor-stimulated PIP3 dynamics in living cells. Importantly, **MFR-K17H** could directly enter and image both inherently enhanced PIP3 levels in breast cancer cells and selective depletion of PIP3 in cancer cells upon treatment with PI3K inhibitors. Finally, the ratiometric response of **DAN-NG-H12G** revealed the organization of PIP3 within nucleolar PIP3 pools, indicating that the acyl chains within the membraneless structure exist in a hydrophobic region.

The advantage of using a peptide-based scaffold for PIP3 detection over a protein scaffold is the ability to fine-tune binding affinity by altering peptide sequences since peptides are easy to design and synthesize. This is aptly highlighted by the observed profound in-cell PIP3 selectivity of our designer probes that was achieved via outwardly minute but strategic changes in lipid-binding peptide sequences guided by detailed analysis of MD simulations and peptide sequence homologies. It is key to note that both high- and low-affinity probes will be essential to access different pools of intracellular PIP3 that are proposed to have different spatiotemporal features. The modular feature of our PIP3 sensor design makes it amenable to easy modifications, which will allow the generation of libraries of PIP3 sensors based on future applications in different PIP3 signaling contexts, as has already been aptly demonstrated with our ability to generate **MFR-K17H** and **DAN-NG-H12G**. Further, our probes can directly report on PIP3 levels both in vitro and in live cells with total experimental times from application of probe to detection within minutes, allowing foreseeable applicability to rapid PIP3 detection assays. **MFR-K17H** and **DAN-NG-H12G** come with a unique combination of cell permeability and the ability to orthogonally image the plasma membrane and nuclear PIP3 pools. These features, unavailable in existing methods of PIP3 detection, should open avenues for exploring yet inaccessible facets of this extremely important lipid.

■ ASSOCIATED CONTENT

Supporting Information

The Supporting Information is available free of charge at https://pubs.acs.org/doi/10.1021/jacsau.3c00738.

Details of molecular dynamics simulations, synthesis, and characterization of the sensors, all in vitro and in-cell experimental procedures, additional control experiment data (PDF)

Video 1. Live tracking of growth factor-induced PIP3 dynamics in living cells using the MFR-K17H sensor. Scale bar, 20 μm (MP4)

Video 2. Imaging cellular uptake of DAN-NG-H12G sensor live. Scale bar, 20 μm (MP4)

■ AUTHOR INFORMATION

Corresponding Author

Ankona Datta − *Department of Chemical Sciences, Tata Institute of Fundamental Research, Mumbai 400005, India;* orcid.org/0000-0003-0821-6044; Email: ankona@tifr.res.in

Authors

Rajasree Kundu − *Department of Chemical Sciences, Tata Institute of Fundamental Research, Mumbai 400005, India;* orcid.org/0000-0001-9704-316X

Sahil Kumar − *Department of Chemical Sciences, Tata Institute of Fundamental Research, Mumbai 400005, India*

Amitava Chandra − *Department of Chemical Sciences, Tata Institute of Fundamental Research, Mumbai 400005, India*

Complete contact information is available at: https://pubs.acs.org/10.1021/jacsau.3c00738

Author Contributions

CRediT: **Rajasree Kundu** conceptualization, data curation, formal analysis, investigation, methodology, validation, writing-original draft; **Sahil Kumar** data curation, investigation; **Amitava Chandra** investigation; **Ankona Datta** conceptualization, data curation, formal analysis, funding acquisition, methodology, project administration, resources, supervision, validation, writing-original draft, writing-review & editing.

Notes

The authors declare no competing financial interest.

■ ACKNOWLEDGMENTS

The authors thank the cell culture facility, confocal facility, and MALDI facility at the Department of Chemical Sciences, TIFR. The authors thank Prof. Ravindra Venkatramani, TIFR, for his intellectual inputs in molecular dynamics simulation analysis, Ms. Sneha Venkatachalapathy for initial peptide-synthesis, and Dr Shamasoddin Shekh for help with DLS. The authors thank: Prof. Roop Mallik's laboratory (IIT Bombay), Prof. Manu Lopus's laboratory (CEBS Mumbai), and Dr. Malay Patra's laboratory (TIFR, Mumbai) for generously sharing COS-7, MDA-MB-231, and MCF-7 cells for experiments and Prof. Krishanu Ray's laboratory (TIFR, Mumbai) for sharing PI3K inhibitors. A.D. acknowledges support from the Department of Atomic Energy, Government of India, under Project Identification No. RTI4003.

■ REFERENCES

(1) Lemmon, M. A. Membrane recognition by phospholipid-binding domains. *Nat. Rev. Mol. Cell Biol.* **2008**, *9* (2), 99−111.
(2) Di Paolo, G.; De Camilli, P. Phosphoinositides in cell regulation and membrane dynamics. *Nature* **2006**, *443* (7112), 651−657.
(3) Posor, Y.; Jang, W.; Haucke, V. Phosphoinositides as membrane organizers. *Nat. Rev. Mol. Cell Biol.* **2022**, *23* (12), 797−816.
(4) Lindsay, Y.; McCoull, D.; Davidson, L.; Leslie, N. R.; Fairservice, A.; Gray, A.; Lucocq, J.; Downes, C. P. Localization of agonist-sensitive PtdIns(3,4,5)P3 reveals a nuclear pool that is insensitive to PTEN expression. *J. Cell Sci.* **2006**, *119* (24), 5160−5168.
(5) Davis, W. J.; Lehmann, P. Z.; Li, W. Nuclear PI3K signaling in cell growth and tumorigenesis. *Front. Cell Dev. Biol.* **2015**, *3*, 24.

(6) Insall, R. H.; Weiner, O. D. PIP3, PIP2, and Cell Movement—Similar Messages, Different Meanings? *Dev. Cell* **2001**, *1* (6), 743−747.
(7) Ridley, A. J.; Schwartz, M. A.; Burridge, K.; Firtel, R. A.; Ginsberg, M. H.; Borisy, G.; Parsons, J. T.; Horwitz, A. R. Cell migration: integrating signals from front to back. *Science* **2003**, *302* (5651), 1704−1709.
(8) Divecha, N.; Irvine, R. F. Phospholipid signaling. *Cell* **1995**, *80* (2), 269−278.
(9) Khan, M. A.; Jain, V. K.; Rizwanullah, M.; Ahmad, J.; Jain, K. PI3K/AKT/mTOR pathway inhibitors in triple-negative breast cancer: a review on drug discovery and future challenges. *Drug Discov. Today* **2019**, *24* (11), 2181−2191.
(10) Dong, C.; Wu, J.; Chen, Y.; Nie, J.; Chen, C. Activation of PI3K/AKT/mTOR Pathway Causes Drug Resistance in Breast Cancer. *Front. Pharmacol.* **2021**, *12*, No. 628690.
(11) Liu, R.; Chen, Y.; Liu, G.; Li, C.; Song, Y.; Cao, Z.; Li, W.; Hu, J.; Lu, C.; Liu, Y. PI3K/AKT pathway as a key link modulates the multidrug resistance of cancers. *Cell Death Dis.* **2020**, *11* (9), 797.
(12) Li, J.; Yen, C.; Liaw, D.; Podsypanina, K.; Bose, S.; Wang, S. I.; Puc, J.; Miliaresis, C.; Rodgers, L.; McCombie, R.; Bigner, S. H.; Giovanella, B. C.; Ittmann, M.; Tycko, B.; Hibshoosh, H.; Wigler, M. H.; Parsons, R. PTEN, a putative protein tyrosine phosphatase gene mutated in human brain, breast, and prostate cancer. *Science* **1997**, *275* (5308), 1943−1947.
(13) Czech, M. P. PIP2 and PIP3: Complex Roles at the Cell Surface. *Cell* **2000**, *100* (6), 603−606.
(14) Wee, P.; Wang, Z. Epidermal Growth Factor Receptor Cell Proliferation Signaling Pathways. *Cancers* **2017**, *9* (5), 52.
(15) Stephens, L. R.; Jackson, T. R.; Hawkins, P. T. Agonist-stimulated synthesis of phosphatidylinositol(3,4,5)-trisphosphate: A new intracellular signalling system? *Biochim. Biophys. Acta Mol. Cell Res.* **1993**, *1179* (1), 27−75.
(16) Lin, A.; Hu, Q.; Li, C.; Xing, Z.; Ma, G.; Wang, C.; Li, J.; Ye, Y.; Yao, J.; Liang, K.; Wang, S.; Park; Peter, K.; Marks; Jeffrey, R.; Zhou, Y.; Zhou, J.; Hung, M.-C.; Liang, H.; Hu, Z.; Shen, H.; Hawke; David, H.; Han, L.; Zhou, Y.; Lin, C.; Yang, L. The LINK-A lncRNA interacts with PtdIns(3,4,5)P3 to hyperactivate AKT and confer resistance to AKT inhibitors. *Nat. Cell Biol.* **2017**, *19* (3), 238−251.
(17) Matsuoka, S.; Ueda, M. Mutual inhibition between PTEN and PIP3 generates bistability for polarity in motile cells. *Nat. Commun.* **2018**, *9* (1), No. 4481.
(18) Salamon, R. S.; Backer, J. M. Phosphatidylinositol-3,4,5-trisphosphate: tool of choice for class I PI 3-kinases. *BioEssays* **2013**, *35* (7), 602−611.
(19) Bunney, T. D.; Katan, M. Phosphoinositide signalling in cancer: beyond PI3K and PTEN. *Nat. Rev. Cancer* **2010**, *10* (5), 342−352.
(20) Costa, C.; Ebi, H.; Martini, M.; Beausoleil, S. A.; Faber, A. C.; Jakubik, C. T.; Huang, A.; Wang, Y.; Nishtala, M.; Hall, B.; Rikova, K.; Zhao, J.; Hirsch, E.; Benes, C. H.; Engelman, J. A. Measurement of PIP3 levels reveals an unexpected role for p110β in early adaptive responses to p110α-specific inhibitors in luminal breast cancer. *Cancer Cell* **2015**, *27* (1), 97−108.
(21) Wymann, M. P.; Schneiter, R. Lipid signalling in disease. *Nat. Rev. Mol. Cell Biol.* **2008**, *9* (2), 162−176.
(22) Vitiello, P. P.; Cardone, C.; Martini, G.; Ciardiello, D.; Belli, V.; Matrone, N.; Barra, G.; Napolitano, S.; Della Corte, C.; Turano, M.; Furia, M.; Troiani, T.; Morgillo, F.; De Vita, F.; Ciardiello, F.; Martinelli, E. Receptor tyrosine kinase-dependent PI3K activation is an escape mechanism to vertical suppression of the EGFR/RAS/MAPK pathway in KRAS-mutated human colorectal cancer cell lines. *J. Exp. Clin. Cancer Res.* **2019**, *38* (1), 41.
(23) Martínez-Sáez, O.; Chic, N.; Pascual, T.; Adamo, B.; Vidal, M.; González-Farré, B.; Sanfeliu, E.; Schettini, F.; Conte, B.; Brasó-Maristany, F.; Rodríguez, A.; Martínez, D.; Galván, P.; Rodríguez, A. B.; Martinez, A.; Muñoz, M.; Prat, A. Frequency and spectrum of PIK3CA somatic mutations in breast cancer. *Breast Cancer Res.* **2020**, *22* (1), 45.
(24) Servant, G.; Weiner, O. D.; Herzmark, P.; Balla, T.; Sedat, J. W.; Bourne, H. R. Polarization of chemoattractant receptor signaling during neutrophil chemotaxis. *Science* **2000**, *287* (5455), 1037−40.
(25) Vidalle, M. C.; Sheth, B.; Fazio, A.; Marvi, M. V.; Leto, S.; Koufi, F. D.; Neri, I.; Casalin, I.; Ramazzotti, G.; Follo, M. Y.; Ratti, S.; Manzoli, L.; Gehlot, S.; Divecha, N.; Fiume, R. Nuclear Phosphoinositides as Key Determinants of Nuclear Functions. *Biomolecules* **2023**, *13* (7), 1049.
(26) Jacobsen, R. G.; Mazloumi Gavgani, F.; Edson, A. J.; Goris, M.; Altankhuyag, A.; Lewis, A. E. Polyphosphoinositides in the nucleus: Roadmap of their effectors and mechanisms of interaction. *Adv. Biol. Regul.* **2019**, *72*, 7−21.
(27) Mazloumi Gavgani, F.; Slinning, M. S.; Morovicz, A. P.; Arnesen, V. S.; Turcu, D. C.; Ninzima, S.; D'Santos, C. S.; Lewis, A. E. Nuclear Phosphatidylinositol 3,4,5-Trisphosphate Interactome Uncovers an Enrichment in Nucleolar Proteins. *Mol. Cell Proteomics* **2021**, *20*, No. 100102.
(28) Kumar, A.; Fernandez-Capetillo, O.; Carrera, A. C. Nuclear phosphoinositide 3-kinase β controls double-strand break DNA repair. *Proc. Natl. Acad. Sci. U.S.A.* **2010**, *107* (16), 7491−7496.
(29) Palmieri, M.; Catimel, B.; Mouradov, D.; Sakthianandeswaren, A.; Kapp, E.; Ang, C.-S.; Williamson, N. A.; Nowell, C. J.; Christie, M.; Desai, J.; Gibbs, P.; Burgess, A. W.; Sieber, O. M. PI3Kα Translocation Mediates Nuclear PtdIns(3,4,5)P3 Effector Signaling in Colorectal Cancer. *Mol. Cell. Proteomics* **2023**, *22* (4), No. 100529.
(30) Yang, J.; Nie, J.; Ma, X.; Wei, Y.; Peng, Y.; Wei, X. Targeting PI3K in cancer: mechanisms and advances in clinical trials. *Mol. Cancer* **2019**, *18* (1), 26.
(31) Blind, R. D.; Sablin, E. P.; Kuchenbecker, K. M.; Chiu, H.-J.; Deacon, A. M.; Das, D.; Fletterick, R. J.; Ingraham, H. A. The signaling phospholipid PIP3 creates a new interaction surface on the nuclear receptor SF-1. *Proc. Natl. Acad. Sci. U.S.A.* **2014**, *111* (42), 15054−15059.
(32) Miao, B.; Skidan, I.; Yang, J.; Lugovskoy, A.; Reibarkh, M.; Long, K.; Brazell, T.; Durugkar, K. A.; Maki, J.; Ramana, C. V.; Schaffhausen, B.; Wagner, G.; Torchilin, V.; Yuan, J.; Degterev, A. Small molecule inhibition of phosphatidylinositol-3,4,5-triphosphate (PIP3) binding to pleckstrin homology domains. *Proc. Natl. Acad. Sci. U.S.A.* **2010**, *107* (46), 20126−20131.
(33) Ananthanarayanan, B.; Ni, Q.; Zhang, J. Signal propagation from membrane messengers to nuclear effectors revealed by reporters of phosphoinositide dynamics and Akt activity. *Proc. Natl. Acad. Sci. U.S.A.* **2005**, *102* (42), 15081−15086.
(34) Hertel, F.; Li, S.; Chen, M.; Pott, L.; Mehta, S.; Zhang, J. Fluorescent Biosensors for Multiplexed Imaging of Phosphoinositide Dynamics. *ACS Chem. Biol.* **2020**, *15* (1), 33−38.
(35) Liu, S. L.; Sheng, R.; O'Connor, M. J.; Cui, Y.; Yoon, Y.; Kurilova, S.; Lee, D.; Cho, W. Simultaneous in situ quantification of two cellular lipid pools using orthogonal fluorescent sensors. *Angew. Chem., Int. Ed.* **2014**, *53* (52), 14387−14391.
(36) Varnai, P.; Bondeva, T.; Tamas, P.; Toth, B.; Buday, L.; Hunyady, L.; Balla, T. Selective cellular effects of overexpressed pleckstrin-homology domains that recognize PtdIns(3,4,5)P3 suggest their interaction with protein binding partners. *J. Cell Sci.* **2005**, *118* (20), 4879−4888.
(37) Várnai, P.; Balla, T. Visualization of phosphoinositides that bind pleckstrin homology domains: calcium- and agonist-induced dynamic changes and relationship to myo-[3H]inositol-labeled phosphoinositide pools. *J. Cell Biol.* **1998**, *143* (2), 501−510.
(38) Várnai, P.; Balla, T. Live cell imaging of phosphoinositide dynamics with fluorescent protein domains. *Biochim. Biophys. Acta* **2006**, *1761* (8), 957−967.
(39) Sharma, A.; Sun, J.; Singaram, I.; Ralko, A.; Lee, D.; Cho, W. Photostable and Orthogonal Solvatochromic Fluorophores for Simultaneous In Situ Quantification of Multiple Cellular Signaling Molecules. *ACS Chem. Biol.* **2020**, *15* (7), 1913−1920.
(40) Sato, M.; Ueda, Y.; Takagi, T.; Umezawa, Y. Production of PtdInsP3 at endomembranes is triggered by receptor endocytosis. *Nat. Cell Biol.* **2003**, *5* (11), 1016−1022.
(41) Kundu, R.; Chandra, A.; Datta, A. Fluorescent Chemical Tools for Tracking Anionic Phospholipids. *Isr. J. Chem.* **2021**, *61* (3−4), 199−216.

https://doi.org/10.1021/jacsau.3c00738
JACS Au 2024, 4, 1004−1017

(42) Yip, S. C.; Eddy, R. J.; Branch, A. M.; Pang, H.; Wu, H.; Yan, Y.; Drees, B. E.; Neilsen, P. O.; Condeelis, J.; Backer, J. M. Quantification of PtdIns(3,4,5)P(3) dynamics in EGF-stimulated carcinoma cells: a comparison of PH-domain-mediated methods with immunological methods. *Biochem. J.* **2008**, *411* (2), 441−448.
(43) Stephens, L.; Eguinoa, A.; Corey, S.; Jackson, T.; Hawkins, P. T. Receptor stimulated accumulation of phosphatidylinositol (3,4,5)-trisphosphate by G-protein mediated pathways in human myeloid derived cells. *EMBO J.* **1993**, *12* (6), 2265−2273.
(44) Hawkins, P. T.; Jackson, T. R.; Stephens, L. R. Platelet-derived growth factor stimulates synthesis of Ptdlns(3,4,5)P3 by activating a Ptdlns(4,5)P2 3-OH kinase. *Nature* **1992**, *358* (6382), 157−159.
(45) Patel, V. B.; Zhabyeyev, P.; Chen, X.; Wang, F.; Paul, M.; Fan, D.; McLean, B. A.; Basu, R.; Zhang, P.; Shah, S.; Dawson, J. F.; Pyle, W. G.; Hazra, M.; Kassiri, Z.; Hazra, S.; Vanhaesebroeck, B.; McCulloch, C. A.; Oudit, G. Y. PI3Kα-regulated gelsolin activity is a critical determinant of cardiac cytoskeletal remodeling and heart disease. *Nat. Commun.* **2018**, *9* (1), No. 5390.
(46) Janmey, P. A.; Lamb, J.; Allen, P. G.; Matsudaira, P. T. Phosphoinositide-binding peptides derived from the sequences of gelsolin and villin. *J. Biol. Chem.* **1992**, *267* (17), 11818−11823.
(47) Liepiņa, I.; Czaplewski, C.; Janmey, P.; Liwo, A. Molecular dynamics study of a gelsolin-derived peptide binding to a lipid bilayer containing phosphatidylinositol 4,5-bisphosphate. *Biopolymers* **2003**, *71* (1), 49−70.
(48) Mondal, S.; Rakshit, A.; Pal, S.; Datta, A. Cell Permeable Ratiometric Fluorescent Sensors for Imaging Phosphoinositides. *ACS Chem. Biol.* **2016**, *11* (7), 1834−1843.
(49) Mondal, S.; Chandra, A.; Venkatramani, R.; Datta, A. Optically sensing phospholipid induced coil−helix transitions in the phosphoinositide-binding motif of gelsolin. *Faraday Discuss.* **2018**, *207*, 437−458.
(50) Henneberry, A. L.; Wright, M. M.; McMaster, C. R. The major sites of cellular phospholipid synthesis and molecular determinants of Fatty Acid and lipid head group specificity. *Mol. Biol. Cell* **2002**, *13* (9), 3148−3161.
(51) Janmey, P. A.; Stossel, T. P.; Allen, P. G. Deconstructing gelsolin: identifying sites that mimic or alter binding to actin and phosphoinositides. *Chem. Biol.* **1998**, *5* (4), R81−R85.
(52) Kucherak, O. A.; Didier, P.; Mély, Y.; Klymchenko, A. S. Fluorene Analogues of Prodan with Superior Fluorescence Brightness and Solvatochromism. *J. Phys. Chem. Lett.* **2010**, *1* (3), 616−620.
(53) Lu, P. J.; Chen, C. S. Selective recognition of phosphatidylinositol 3,4,5-trisphosphate by a synthetic peptide. *J. Biol. Chem.* **1997**, *272* (1), 466−472.
(54) Chan, T. O.; Rittenhouse, S. E.; Tsichlis, P. N. AKT/PKB and Other D3 Phosphoinositide-Regulated Kinases: Kinase Activation by Phosphoinositide-Dependent Phosphorylation. *Annu. Rev. Biochem.* **1999**, *68* (1), 965−1014.
(55) Kallergi, G.; Agelaki, S.; Kalykaki, A.; Stournaras, C.; Mavroudis, D.; Georgoulias, V. Phosphorylated EGFR and PI3K/Akt signaling kinases are expressed in circulating tumor cells of breast cancer patients. *Breast Cancer Res.* **2008**, *10* (5), R80.
(56) Freudlsperger, C.; Burnett, J. R.; Friedman, J. A.; Kannabiran, V. R.; Chen, Z.; Van Waes, C. EGFR-PI3K-AKT-mTOR signaling in head and neck squamous cell carcinomas: attractive targets for molecular-oriented therapy. *Expert Opin. Ther. Targets* **2011**, *15* (1), 63−74.
(57) Díaz, M. E.; González, L.; Miquet, J. G.; Martínez, C. S.; Sotelo, A. I.; Bartke, A.; Turyn, D. Growth hormone modulation of EGF-induced PI3K-Akt pathway in mice liver. *Cell Signal.* **2012**, *24* (2), 514−523.
(58) Qiao, M.; Sheng, S.; Pardee, A. B. Metastasis and AKT activation. *Cell Cycle* **2008**, *7* (19), 2991−2996.
(59) Yavas, S.; Macháň, R.; Wohland, T. The Epidermal Growth Factor Receptor Forms Location-Dependent Complexes in Resting Cells. *Biophys. J.* **2016**, *111* (10), 2241−2254.
(60) Wang, Y.; Gao, J.; Guo, X.; Tong, T.; Shi, X.; Li, L.; Qi, M.; Wang, Y.; Cai, M.; Jiang, J.; Xu, C.; Ji, H.; Wang, H. Regulation of EGFR nanocluster formation by ionic protein-lipid interaction. *Cell Res.* **2014**, *24* (8), 959−976.
(61) Li, Y.-p.; Mikrani, R.; Hu, Y.-f.; Faran Ashraf Baig, M. M.; Abbas, M.; Akhtar, F.; Xu, M. Research progress of phosphatidylinositol 4-kinase and its inhibitors in inflammatory diseases. *Eur. J. Pharmacol.* **2021**, *907*, No. 174300.
(62) Idevall-Hagren, O.; Dickson, E. J.; Hille, B.; Toomre, D. K.; De Camilli, P. Optogenetic control of phosphoinositide metabolism. *Proc. Natl. Acad. Sci. U.S.A.* **2012**, *109* (35), E2316−E2323.
(63) Foki, E.; Stanisz, I.; Kadletz, L.; Kotowski, U.; Seemann, R.; Schmid, R.; Heiduschka, G. HS-173, a selective PI3K inhibitor, induces cell death in head and neck squamous cell carcinoma cell lines. *Wien. Klin. Wochenschr.* **2021**, *133* (1), 26−31.

https://doi.org/10.1021/jacsau.3c00738
JACS Au 2024, 4, 1004−1017